Available online at www.sciencedirect.com
ScienceDirect
Electrochimica Acta 51 (2006) 6251–6257
ELECTROCHIMICA Acta
www.elsevier.com/locate/electacta

Copper nanowires within the central channel of tobacco mosaic virus particles

S. Balci [a], A.M. Bittner [a,*], K. Hahn [b], C. Scheu [b,1], M. Knez [a,2], A. Kadri [c], C. Wege [c], H. Jeske [c], K. Kern [a]

[a] *Max-Planck-Institut für Festkörperforschung, Heisenbergstr. 1, D-70569 Stuttgart, Germany*
[b] *Max-Planck-Institut für Metallforschung, Heisenbergstr. 3, D-70569 Stuttgart, Germany*
[c] *Biologisches Institut, Universität Stuttgart, Pfaffenwaldring 57, D-70550 Stuttgart, Germany*

Received 8 March 2006; accepted 6 April 2006
Available online 19 May 2006

Abstract

Simple electrochemical deposition techniques can produce highly defined metal nanostructures in templates. Electroless deposition (ELD) can be effectively used for depositing metals on insulators such as biological or plastic surfaces. With biomolecular templates, metallization methods are often restricted to mild reductions, and the deposition of copper at pH values above 12 is usually not applicable. We produced copper nanowires of 3 nm in diameter and up to 150 nm in length by electroless deposition within the 4 nm wide channel of tobacco mosaic virus (TMV) particles. We employed a low pH (∼7.5) copper electroless deposition solution that is compatible with biomolecules. The fabrication process of the nanowires is based on sensitization of tobacco mosaic virus with Pd(II) prior to the electroless deposition. We analyzed the chemical composition of the nanowires by energy-filtering transmission electron microscopy, and used the method also for nickel and cobalt nanowires deposited within the viral channel.

Keywords: Tobacco mosaic virus; Electroless deposition; Template; Cu nanowires; Energy-filtering TEM

1. Introduction

The size of features on integrated circuits has rapidly decreased, due to the improvements in the lithographic materials and techniques used to fabricate microstructures. However, fabrication of nanostructures (below 100 nm) with optical patterning techniques remains problematic mainly due to the ambient absorption of hard ultraviolet radiation and expensive instrumentation required. An alternative method is a bottom-up, or self-assembly, strategy, which uses chemical or physical forces operating at the nanoscale to assemble basic units into larger structures [1]. As component size decreases in nanofabrication (below 100 nm), bottom-up approaches provide an increasingly important complement to top-down techniques. One potential bottom-up method involves using biological molecules as templates for arranging and producing circuit components. Rod- or tube-like biological molecules, such as DNA [2], tobacco mosaic virus (TMV) [3,4], bacteriophages [5], protein tubes [6] and protein fibers [7,7a] are well defined in their chemical composition and structure. Such molecules are used as templates for the nucleation of nanoscale inorganic structures [2–22].

Here we present the synthesis of copper nanowires of 3 nm in diameter with electroless deposition within the 4 nm wide channel of TMV particles. Galvanic copper deposition has become very popular after the invention of "damascene" copper electrodeposition (embedded copper technology) for on-chip metallization. Advantages – compared to the formerly used aluminum – are decreased resistance, improved reliability and reduced process complexity [23]. Biotemplates normally cannot be contacted electrically; therefore electroless deposition (ELD) is favored over electrodeposition. In addition, ELD is advantageous for high-aspect ratio structures since they can be filled or decorated without clogging up or closing an orifice [24]. Our

* Corresponding author. Tel.: +49 711 689 1433; fax: +49 711 689 1079.
E-mail address: a.bittner@fkf.mpg.de (A.M. Bittner).
[1] Present Address: Department Physical Metallurgy and Materials Testing, University of Leoben, Franz-Josef-Str. 18, A - 8700 Leoben, Austria.
[2] Present Address: Max-Planck-Institut für Mikrostrukturphysik, Weinberg 2, D-06120 Halle, Germany.

0013-4686/$ – see front matter © 2006 Elsevier Ltd. All rights reserved.
doi:10.1016/j.electacta.2006.04.007

template, TMV, is rod-shaped, 300 nm long and 18 nm in diameter, with a central channel diameter of 4 nm [22]. The exact amino acid sequence of the TMV coat protein is known, and thus one can induce regioselective covalent linking [19,20] or localized chemical reactions with metal ions [3,4,9,13].

"Sensitization" ("activation") [3,8,9,24–28] creates noble metal clusters on nonconductive surfaces. The details of this pretreatment are not yet known even though some theoretical studies exist [10,29]. Followed by ELD, the two-step process is comparable to the "enhancement" of latent photographic patterns. We sensitized a TMV suspension with noble metal complexes such as Pt(II) or Pd(II); only very small clusters (<1 nm diameter) are formed during this procedure [9]. The TMV suspension was then washed and mixed with the ELD solution containing metal ions, complexants and a reductant (e.g. Cu(II), EDTA and a borane-containing reductant). As usual in ELD, the deposition starts, at first catalyzed by the noble metal nanoparticles. Later, the deposited metal catalyzes its own reductive deposition; therefore the metal particles can continue to grow. In this way, we had already synthesized nickel and cobalt nanowires in the inner channel of TMV particles with ELD [9]. An extension to copper is not straightforward, especially for biotemplates. For example, Demir et al. [19] have reported the photo-reduction of copper at the outer surface (coat) of TMV particles at pH 6.5, and found a relatively low number of polydisperse copper particles. Monson and coworkers have developed a method to deposit copper metal onto surface-attached DNA, forming nanowire-like structures that are ∼3 nm in diameter; however, some copper complexes cleave DNA molecules and produce short DNA molecules, which results in short copper nanowires (10 nm in length) [21]. Therefore, DNA is not an optimal template for fabricating long copper nanowires with a very small diameter.

Copper ELD usually entails very high pH values (up to 13) [24,25], which are incompatible with most biomolecules; therefore we used a low-pH (∼7.5) copper ELD solution that contains – as nearly all ELD solutions – a reductant, a metal ion source, a complexing agent and a buffering agent. The buffering agent controls the pH during ELD, which is very important for the deposition of metals on virions since already moderately high pH values (>9) can denature the viral coat proteins [22]. The complexing agent, preventing random deposition of metal ions in the solution, changes the electrochemical reduction potential of the corresponding metal ions and determines the stability of the ELD solution [24,25]. The reductant reduces the metal ions in the ELD solution to the metallic state. In order to develop a new ELD solution for the deposition of metals on biomolecular surfaces, all the parameters, such as concentration of the components in the deposition solution, pH value and temperature of the deposition solution, have to be compatible with the corresponding surfaces.

In the present work we also apply energy-filtering transmission electron microscopy (EFTEM) to investigate the copper, nickel, and cobalt nanowires in the inner channel of TMV. Energy-filtering transmission electron microscopy is a powerful tool for nanoanalytical studies. It allows the analysis of small specimen volumes with high sensitivity and resolution in the nanometer range, using the information provided by inelastically scattered electrons in a spatially resolved manner [30–32]. The method uses the characteristic inner-shell energy-loss edges of the element under study for mapping the elemental distribution over small areas with a resolution in the nanometer range [30,31]. By elemental mapping, EFTEM was used for chemical analysis of several different nanomaterials: Grobert et al. [33] have reported a nickel/iron alloy (invar) inside carbon nanotubes and Reis et al. [16] have reported FePt nanoparticles on the M13 bacteriophage.

2. Experimental

2.1. TMV isolation

A Plasmid-DNA was employed to mechanically infect *Nicotiana tabacum* cv. Samsun nn plants (see also ref. [3] for details of the virus preparation). TMV particles were isolated from systemically infected leaves 4 weeks post inoculation [3]. Differential centrifugation including density gradient was employed for virus isolation, yielding 6 mg TMV/g plant material. The virus suspension was stored in phosphate buffer (pH 7.4) at 4 °C. It was dialyzed before metallization using Slide-A-Lyzer 10000 MWCO units (KMF, Lohmar).

2.2. Deposition of metals

Before metallization, the TMV suspension was first sensitized with aqueous Pd(II). 500 μl of a 0.2 mg/ml TMV suspension in water was incubated with the same amount of freshly prepared aqueous 1.36 mM Na_2PdCl_4 (Aldrich, 99.998%) with excess (1M) NaCl (Merck, ≥99.5%) at pH 5.0. After 10 min, the suspension was centrifuged for 10 min at 14000 rpm, producing a pale brown pellet. The supernatant was removed and the pellet washed twice with water by resuspension and repeated centrifugation. Pd(II)-incubated TMV suspension was metallized with copper by treating the virus suspension with the corresponding copper electroless deposition (ELD) solution for 20–30 min (second step). In analogy to other electroless deposition reactions based on DMAB (dimethylamine borane), gas bubbles formed during the reaction.

The ELD copper solution described by Jagannathan et al. was used in order to metallize TMV with copper at lower pH level (pH ∼7.5) [28]. Pd (II)-incubated TMV suspension was mixed with an equal volume of a solution containing 0.032 M $CuSO_4{\cdot}5H_2O$ (Sigma, 99.999%), 0.04 M Na_2H_2EDTA (ethylenediaminetetraacetic acid disodium salt, Aldrich), 0.05 M TEA (triethanolamine, Janssen Chimica, 97%), and 0.067 M DMAB (Aldrich, 97%) in water. All metallization steps were carried out at room temperature. Water was purified with a Millipore Milli-Q or a Barnstead Nanopure apparatus to 18.2 MΩcm. For nickel wire production, Pd(II)-incubated TMV suspension was metallized by mixing the suspension with an equal volume of a solution containing 0.18 M $Ni(CH_3COO)_2{\cdot}4H_2O$ (Aldrich, 98%), 0.23 M lactic acid (Aldrich, 95%) and 0.067 M DMAB (Aldrich, 97%). For cobalt metallization (see Fig. 2c for the nanowire), the Pd(II)-incubated

TMV suspension was mixed with an equal volume of a solution containing 0.14 M $CoSO_4 \cdot H_2O$ (Aldrich), 0.15 M sodium succinate (Aldrich, 99%) and 0.067 M DMAB. Metallization times were as for copper.

2.3. Sample preparation

In order to analyze the chemical composition of nanowires by EFTEM, 10 μl aliquots of the TMV suspension were taken directly from the respective metallization bath, deposited on formvar/carbon-coated copper grids (300 or 400 mesh, SPI-Supplies), and incubated for 2–3 min, after which the suspension was wicked off with a filter paper. Prior to the deposition of the metallized virions, the grids were dipped into ethanol (Roth Rotipuran, ≥99.8%) and air-dried.

2.4. Energy-filtering transmission electron microscopy measurements

The specimens were investigated by EFTEM in order to study the nanometer chemical composition of nanowires. All experiments were performed on a Zeiss 912 Omega energy-filtering microscope operated at 120 kV, except for Fig. 1 where a Philips CM 200 at 200 kV (photographic detection) was used. The Zeiss TEM data were acquired using a Gatan slow scan CCD camera with 1024 × 1024 pixels and 25 μm pixel size. For the experiments a window size of 50 eV, binning 2x, an objective aperture of 60 μm and an exposure time of 60 s for each image were used. The copper map was calculated using two pre-edge images and one post-edge image at 841, 901 and 961 eV, respectively, by using the three-window technique. In the same way, a nickel map was recorded with two pre-edge images and a post-edge image at 775, 820 and 885 eV. For cobalt, 699, 749 and 804 eV were used. An integration width of 20 pixels, corresponding to 19.5 nm box length (parallel to the nanowire), was used for all line profiles. We tried to operate the Zeiss 912 microscope at 60 kV instead of the usual 120 kV to obtain a better contrast for the virions, but the data did not improve.

3. Results and discussion

3.1. Deposition of copper

In order to deposit copper, first we tested standard formaldehyde-based high pH level ELD solutions [23–25], but found that the virions were destroyed since TMV denatures at pH >9 [22]. In order to deposit metal on biological surfaces, all reactions and components in the deposition solution have to be compatible with the template (pH, deposition rate, temperature, . . .). For instance, the pH of the deposition solution often has to be maintained around ∼7 to avoid denaturation of proteins—in our case to avoid disassembly of the protein subunits during deposition. In addition, we also require a highly selective deposition of metals on biological surfaces without deposition in the bulk solution or the enclosing reaction vessel. In order to fulfill all the requirements for copper deposition on the nanoscale within the TMV central cavity, we used the copper deposition solution described by Jagannathan and Krishnan [28]. After their initial studies with EDTA-based systems, the authors focused on multidentate nitrogen donors that form very strong complexes with copper. In this way one can increase the stability of the ELD solution at pH ∼9. However, we switched back to EDTA as the complexing agent in our deposition solution (pH ∼7.5), since we found that the solution can be stored for long times without special protection. The other ingredients in the process were copper sulfate as the metal ion source, triethanolamine as the buffering agent, and DMAB as the reducing agent. DMAB is a strong reducing agent, which operates especially well at basic pH values [28,34]. A buffer, here TEA, is essential since the electroless metal deposition as well as side reactions of DMAB (see below) consume OH^-, which would decrease the pH of the solution and thus decrease the deposition rate.

After activation of the virus particles with a catalyst (Pd(II)), the metallization bath resulted in deposition of copper within the 4 nm-wide internal channel of TMV particles without denaturation of the virus particles. Fig. 1a and b show bright-field transmission electron microscopy (TEM) images of copper

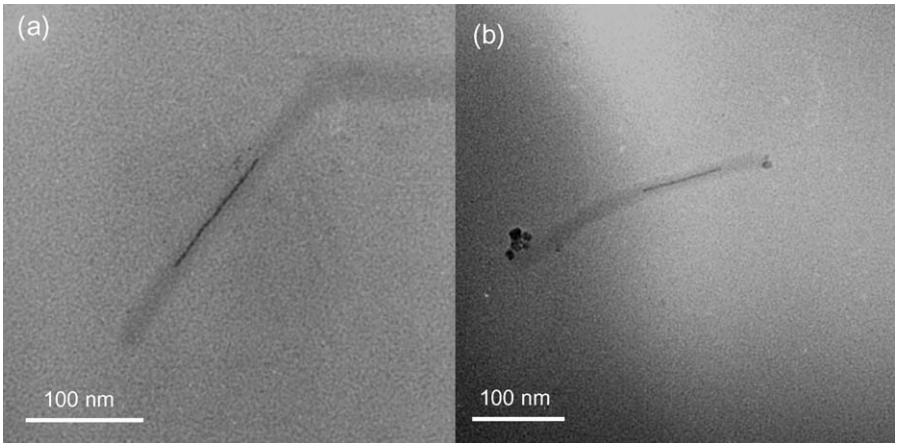

Fig. 1. TEM micrograph of copper nanowires within the central channel of TMV particles. (a) The dark line corresponds to a copper nanowire, 3 nm in diameter, and 115 nm in length. The wire is surrounded by dark-grey region, the viral coat proteins of two end-to-end aggregated virions, of which only one is metallized. (b) A 85 nm copper nanowire (dark line 3 nm in diameter) within the central channel of a virion (grey region around the nanowire).

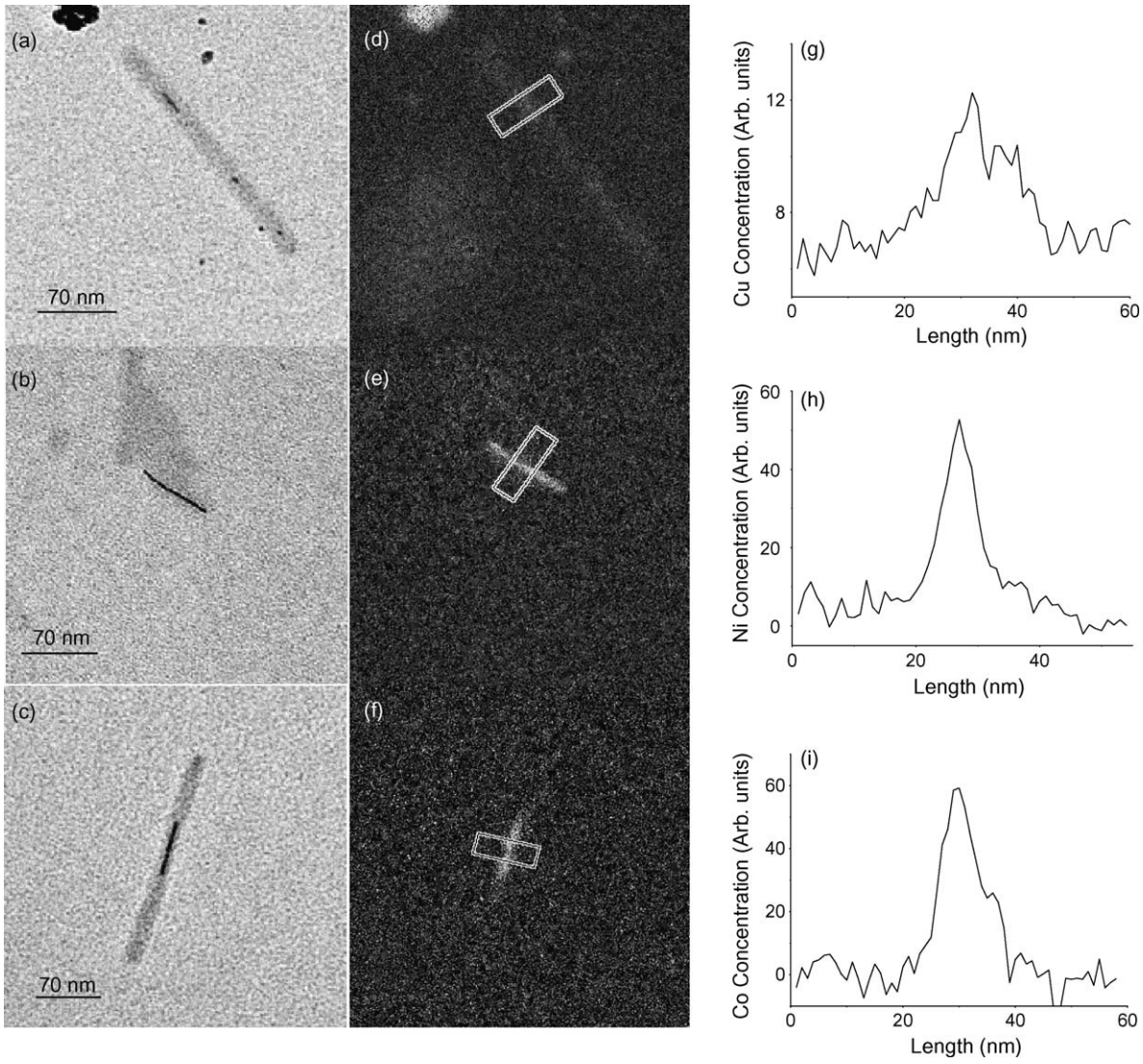

Fig. 2. Elemental mapping of copper, nickel and cobalt nanowires by EFTEM. A bright field TEM image of (a) copper, (b) nickel, and (c) cobalt nanowires within the central channel of TMV particles and the corresponding elemental distribution images ((d) copper, (e) nickel, and (f) cobalt) recorded with the three-window technique (Cu $L_{2,3}$ edge at 931 eV, Ni $L_{2,3}$ edge at 854 eV, and Co $L_{2,3}$ edge at 779 eV). Line profiles integrated over 20 pixels (19.5 nm) show the compositional line traces of the elements inside the marked areas ((g) copper, (h) nickel, and (i) cobalt).

nanowires in virions, ~3 nm in diameter. Therefore, electroless deposition can also be used on the nanoscale (below 5 nm) for the generation of materials. The exact diameter of the nanowire is difficult to measure since the borders of the wire are not always clearly visible. In four separate experiments, we observed that between 40 and 50% of the TMV particles were metallized with copper, and that the length of the wires varied from 5 to 150 nm. We never found a 300 nm long copper wire within the virus central channel.

The ELD of copper can be formulated as follows, assuming complete oxidation of the borane [35,38], and taking into account the various (de)protonation equilibria:

$$4(CH_3)_2NHBH_3 + 12CuEDTA^{2-} + 9OH^- \rightarrow HB_4O_7^- + 12Cu + 4(CH_3)_2NH_2^+ + 12HEDTA^{3-} + 2H_2O \quad (1)$$

The equilibrium is on the right hand side, hence ELD of copper is thermodynamically allowed (spontaneous reaction); the kinetic barrier is so high that spontaneous deposition does not occur in the deposition bath [25], and catalysts such as noble metals (or copper) are required. The Pourbaix diagram for the system boron-water shows that $HB_4O_7^-$ is the dominant species at pH values from seven to nine at nearly all relevant redox potentials (from −1.0 to 0.8 V) [35]. Note that the (formal) oxidation state of the boron does not change: the hydrogen atoms are oxidized. The reaction can be separated into two-half reactions, cathodic reduction of copper ions and anodic oxidation of DMAB on a catalytic surface such as palladium for the first copper atoms to be deposited, or copper during ELD [25,36-38]. The reduction of the copper-EDTA complex

$$2e^- + CuEDTA^{2-} + H_2O \rightarrow Cu^0 + OH^- + HEDTA^{3-} \quad (2)$$

requires potentials below $-0.22\ V_{SHE}$ [25]. Note that the formation constant of the complex is very high (log $K_f = 18.8$), thus

free Cu^{2+} is practically absent [25]. We assume that the oxidation of DMAB is described by

$$4(CH_3)_2NHBH_3 + 21OH^- \rightarrow HB_4O_7^- + 4(CH_3)_2NH_2^+ + 14H_2O + 24e^- \quad (3)$$

which is a two-electron process (per H atom of the borane) [38]. Note that this equation does not suggest any mechanism. When the oxidation is combined with nickel or cobalt ion reduction, the mixed potential is around −700 to −600 mV_{SHE} [37], well compatible with the onset of DMAB oxidation on gold at roughly −700 mV_{SHE} for our pH value, 7.5 [38]. Obviously, the reduction of the more noble copper compounds is allowed. However, the mechanism of the anodic oxidation of DMAB has not been completely clarified and depends strongly on the pH value [25,36–38]. There appears to be general agreement that $BH_3(OH)^-$ is the active reducing species—clearly its formation from DMAB depends on pH. Multistep electron transfers that each involves the production of hydrogen (one-electron oxidation of the borane hydrogen atoms) have been proposed for alkaline media [25,34]:

$$2BH_{4-n}(OH)_n^- + 2OH^- \rightarrow 2BH_{3-n}(OH)_{1+n}^- + H_2 + 2e^- \quad (4)$$

(with $n = 1,2,3$ in the course of the oxidation). This mechanism predicts a strong correlation with high pH values; hence it cannot be expected to be valid at pH values around 7. The relevant redox potentials have been determined at several very basic pH values [34]. An extrapolation of the pH dependence to our pH 7.5 gives values above 0 V_{SHE}, which would not allow copper, let alone cobalt or nickel reduction, another indication that the multistep mechanism (4) can be responsible only for side reactions, especially hydrogen evolution. This would explain the observed gas bubbles. In passing we note that all mechanisms can involve the codeposition of boron in the metal structure during yet another side reaction [36], with important consequences for mechanical and magnetic properties of the deposit.

While all these considerations are valid for the macroscopic scale, nanoscale ELD can change a number of parameters. For example, the dissolution potential of nanoscale metals can shift some mV from the bulk value [39]. The concentrations in the vicinity of a growing copper surface deviate substantially from bulk values. In the extreme case, one may have to be cautious to define concentrations: a 4 nm long part of the 4 nm wide channel of TMV contains only one copper ion and two DMAB molecules, and the electrochemical double layer on the face of a growing copper wire refers to an area of only $\pi(2\,nm)^2$ with 220 copper atoms.

The ELD of copper within the central channel of virions consists of several steps, each of which should be carefully analyzed. Crucially important is the surface chemistry of TMV: in the case of virions stored in phosphate buffer, the TMV suspension is dialyzed against water prior to usage, because metallization occurs on the exterior surface of the virions due to adsorbed phosphate [3]. Our sensitization solution contains only Na_2PdCl_4 (1.36 mM) and excess NaCl (1 M) at pH 5, aiming to deposit metals within the hollow channel of TMV particles. Excess NaCl is very important in order to avoid formation of palladium oxo and hydroxo complexes [26], which is favored when the pH value is above two and when the chloride concentration is very low. In order to initiate deposition of metals within the central channel of TMV, the palladium complex has to reach the central channel of the virion. It cannot bind electrostatically to the negatively charged channel [13], however, it might form complexes with the functional groups of amino acids (for example lysine, arginine, asparagine) lining the interior channel, even when the residues contain positively charged protonated amine groups [26]. Prior to the ELD of copper, the Pd(II) species have to be reduced by the reductant (DMAB) since only Pd^0 can act as a catalyst for ELD, but not Pd(II). Since small palladium (or platinum) clusters down to a few atoms in size are catalytically active [10,26], and the inside surface of TMV has to be coated uniformly with the palladium clusters rather than totally filled with them, the copper deposition can not only be confined to the viral channel, but also be so effective that the channel is filled with a wire instead of separate clusters.

3.2. Deposition of nickel and cobalt

Nickel and cobalt nanowires were produced [9], again within the central channel of TMV particles, after ELD of Pd(II)-sensitized TMV suspension with special ELD formulations (see also Section 2 for details). ELD mechanisms and redox potentials have been discussed above; here we mention that nickel and cobalt require more negative mixed potentials that are still above the onset of the two-electron oxidation of DMAB. Fig. 2b and c show bright-field TEM images of nickel and cobalt nanowires (dark lines), respectively. The diameter of the nickel nanowires is ∼3 nm, and their length ∼65 nm, as determined from the respective images. The grey-shaded region around the nickel wire is interpreted to represent a destroyed TMV particle, distributed on the carbon-coated TEM grid. The dark cobalt nanowire within the single TMV particle (grey-shaded region around the nanowire) shown in Fig. 2c exhibits similar dimensions as the nickel wire in Fig. 2b. Cobalt wires of similar diameter were recently reported by Kazakova et al. [40].

3.3. Chemical analysis of nanowires

The electron spectroscopic image revealing the copper elemental distribution is displayed in Fig. 2d, which was obtained using the element-specific signal at the Cu $L_{2,3}$ edge at 931 eV and two pre-edge images for background subtraction. Fig. 2g shows the corresponding integrated line profile from the box-shaped area indicated in Fig. 2d. Fig. 2b, e and h are the corresponding images and elemental maps for nickel (Ni $L_{2,3}$ edge at 854 eV), while Fig. 2c, f and i refer to cobalt (Co $L_{2,3}$ edge at 779 eV). In addition to the measurements from the bright-field images, the diameters of the copper, nickel, and cobalt nanowires were also determined from the corresponding integrated line profiles (Fig. 2g–i). The full width at half maximum (FWHM) values in the integrated line profiles for the copper, nickel, and cobalt nanowires are 13.5, 7.8, and 7.1 nm, respectively. These

FWHM values are higher than the ∼3 nm determined from bright-field TEM images. Most likely this difference is due to instrumental drift during the EFTEM measurements, and also due to noise problems especially for the copper nanowires, as will be discussed further below. In principle, the intensity of elemental maps can be increased by using longer acquisition times and/or a higher beam current. However, longer acquisition times resulted in an even more pronounced drift of the samples during the acquisition of the pre-edge and post-edge images, leading to artefacts in the calculated elemental map. Measurements with higher beam currents have the disadvantage that the nanowires are damaged, again causing artefacts.

As mentioned above, the line profile intensity of the copper nanowires shows lower counts than the nickel and cobalt line profile intensity. The width of the profile (FWHM) is not only larger than in the bright-field image, it is also larger than for cobalt and nickel. For nickel and cobalt, sharp white lines occur at the edge onset due to the excitation of 2p electrons into unoccupied 3d states [31,32] (see Fig. 3). In contrast, no pronounced features occur at the Cu $L_{2,3}$ edge since the 3d shell is fully occupied [32] (Fig. 3). In addition, the Cu $L_{2,3}$ edges lies at the highest energy-loss (931 eV) in the investigated materials, and thus the intensity of this edge is lowest [31,32] (see Fig. 3). Due to these reasons, the intensity in the elemental maps for copper is lower than for nickel and cobalt, if all other parameters (acquisition time and beam current) are the same. The diminished signal/noise ratio increases the FWHM, thus making EFTEM analysis of copper nanostructures comparatively difficult. Accordingly, the FWHM value determines the resolution of the chemical information, while the structural resolution from the TEM image is considerably better (FWHM ∼4 nm). We also performed measurements using a scanning transmission electron microscope (VG HB 501 UX operated at 100 kV), which is capable to form an electron probe with a size of less than 1 nm. It has a higher spatial resolution for analytical measurements compared to the TEM used for the EFTEM investigations, however, due to the high electron beam current density radiation damage occurred at the nanowires. The results are thus omitted here.

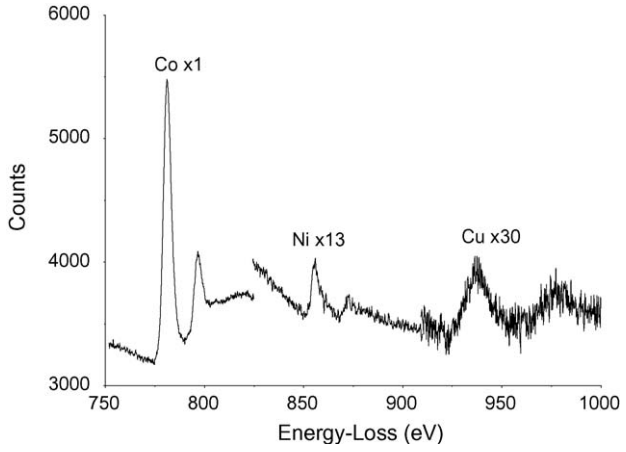

Fig. 3. Comparison of the $L_{2,3}$ white lines of cobalt with nickel and copper electron energy-loss spectra. The nickel and copper signals are enlarged by the indicated factors.

4. Conclusion

In this work it is shown that copper electroless deposition can be used to synthesize nanosized copper wires specifically within the central channel of TMV particles, 3 nm in diameter and up to 150 nm in length. Therefore, electroless deposition methods can also be useful for nanotechnology applications. We employed electroless copper deposition solution at physiological conditions (pH ∼7.5) that is compatible with biomolecules. The fabrication process of the nanowires is based on treatment of TMV with Pd(II), followed by electroless deposition of copper. Energy-filtering transmission electron microscopy proves that the copper nanowires synthesized with the method of ELD within the 4 nm central channel of TMV particles are indeed composed of copper. In addition, a similar proof was obtained also for nickel and cobalt nanowires. Length and diameter of the elemental maps of all three metal wires reproduce the respective bright field TEM images. A closer analysis of the widths of the EFTEM features shows a dependence on the metal: copper, nickel, and cobalt have FWHM values of 13.5, 7.8, and 7.1 nm, respectively. The sensitivities for cobalt and nickel are higher than for copper in elemental maps since copper spectra do not possess sharp "white lines" in the energy-loss spectra, and the Cu $L_{2,3}$ edge lies at the highest energy of the materials investigated as well.

Appendix A. Supplementary data

Supplementary data associated with this article can be found, in the online version, at doi:10.1016/j.electacta.2006.04.007.

References

[1] G.M. Whitesides, J.P. Mathias, C.T. Seto, Science 254 (1991) 1312.
[2] E. Braun, Y. Eichen, U. Sivan, G. Ben-Yoseph, Nature 391 (1998) 775.
[3] M. Knez, M. Sumser, A.M. Bittner, C. Wege, H. Jeske, T.P. Martin, K. Kern, Adv. Funct. Mater. 14 (2004) 116.
[4] W. Shenton, T. Douglas, M. Young, G. Stubbs, S. Mann, Adv. Mater. 11 (1999) 253.
[5] C. Mao, D.J. Solis, B.D. Reiss, S.T. Kottmann, R.Y. Sweeney, A. Hayhurst, G. Georgiou, B. Iverson, A.M. Belcher, Science 303 (2004) 213.
[6] M. Reches, E. Gazit, Science 300 (2003) 625.
[7] M. Mertig, R. Kirsch, W. Pompe, Appl. Phys. A 66 (1998) S723.
[7a] T. Scheibel, R. Parthasarathy, G. Sawicki, X.M. Lin, H. Jaeger, S.L. Lindquist, PNAS 100 (2003) 4527.
[8] A.M. Bittner, Naturwissenschaften 92 (2005) 51.
[9] M. Knez, A.M. Bittner, F. Boes, C. Wege, H. Jeske, E. Maib, K. Kern, Nano Lett. 3 (2003) 1079.
[10] M. Mertig, L.C. Ciacchi, R. Seidel, W. Pompe, Nano Lett. 2 (2002) 841.
[11] M. Mertig, R. Wahl, M. Lehmann, P. Simon, W. Pompe, Eur. Phys. J. D. 16 (2001) 317.
[12] J. Richter, M. Mertig, W. Pompe, I. Mönch, H.K. Schackert, Appl. Phys. Lett. 78 (2001) 536.
[13] E. Dujardin, C. Peet, G. Stubbs, J.N. Culver, S. Mann, Nano Lett. 3 (2003) 413.
[14] Q. Wang, T. Lin, L. Tang, J.E. Johnson, M.G. Finn, Angew. Chem. Int. Ed. 41 (2002) 459.
[15] Z. Deng, C. Mao, Nano Lett. 3 (2003) 1545.
[16] B.D. Reiss, C. Mao, D.J. Solis, K.S. Ryan, T. Thomson, A.M. Belcher, Nano Lett. 4 (2004) 1127.

[17] J.C. Falkner, M.E. Turner, J.K. Bosworth, T.J. Trentler, J.E. Johnson, T. Lin, V.L. Colvin, J. Am. Chem. Soc. 127 (2005) 5274.
[18] K. Keren, R.S. Berman, E. Buchstab, U. Sivan, E. Braun, Science 302 (2003) 1380.
[19] M. Demir, M.H.B. Stowell, Nanotechnology 13 (2003) 541.
[20] T.L. Schlick, Z. Ding, E.W. Kovacs, M.B. Francis, J. Am. Chem. Soc. 127 (2005) 3718.
[21] C.F. Monson, A.T. Woolley, Nano Lett. 3 (2003) 359.
[22] M. Zaitlin, AAB Descriptions of Plant Viruses 8 (2000) 370.
[23] P.C. Andricacos, C. Uzoh, J.O. Dukovic, J. Horkans, H. Deligianni, IBM. J. Res. Dev. 42 (1998) 567.
[24] Y. Shacham-Diamand, V. Dubin, M. Angyal, Thin Solid Films 262 (1995) 93.
[25] M. Schlesinger, M. Paunovic, Modern electroplating, John Wiley & Sons, Inc., New York, 2000.
[26] H. Kind, A.M. Bittner, O. Cavalleri, K. Kern, J. Phys. Chem. B 102 (1998) 7582.
[27] E.A. Dobisz, R. Bass, S.L. Brandow, M.S. Chen, W. Dressick, J. Appl. Phys. Lett. 82 (2003) 478.
[28] R. Jagannathan, M. Krishnan, IBM. J. Res. Dev. 37 (1993) 117.
[29] H. Nakai, T. Homma, I. Komatsu, T. Osaka, J. Phys. Chem. B 105 (2001) 1701.
[30] A. Berger, H. Kohl, Microsc. Microanal. Microstruct. 3 (1992) 159.
[31] D.B. Williams, C.B. Carter, Transmission electron microscopy, Plenum Press, New York and London, 1996.
[32] R.D. Leapman, L.A. Grunes, P.L. Fejes, Phys. Rev. B 26 (1982) 614.
[33] N. Grobert, M. Mayne, M. Terrones, J. Sloan, R.E. Dunin-Borkowski, R. Kamalakaran, T. Seeger, H. Terrones, M. Rühle, D.R.M. Walton, H.W. Kroto, J.L. Hutchison, Chem. Commun. (2001) 471.
[34] O.A. Sadik, H. Xu, A. Sargent, J. Electroanal. Chem. 583 (2005) 167.
[35] M. Pourbaix, Atlas of electrochemical equilibria in aqueous solutions, National association of corrosion engineers, Texas, 1966.
[36] Y. Sverdlov, V. Bogush, H. Einati, Y. Shacham-Diamand, J. Electrochem. Soc. 152 (2005) C631.
[37] T. Saito, E. Sato, M. Matsuoka, C. Iwakura, J. Appl. Electrochem. 28 (1998) 559.
[38] L.D. Burke, B.H. Lee, J. Appl. Electrochem. 22 (1992) 48.
[39] D.M. Kolb, R. Ullmann, T. Will, Science 275 (1997) 1097.
[40] O. Kazakova, D. Erts, T.A. Crowley, J.S. Kulkarni, J.D. Holmes, J. Magn. Magn. Mater. 286 (2005) 171.